SUPPORTING INFORMATION

Amelogenin phosphorylation regulates tooth enamel formation by stabilizing a transient amorphous mineral precursor

Nah-Young Shin[1,2,%], Hajime Yamazaki[1,2,3#], Elia Beniash[3], Xu Yang[3], Seth S. Margolis[4], Megan K. Pugach[1,2], James P. Simmer[5] and Henry C. Margolis[1, 2, 6, &*]

From the [1]The Forsyth Institute, Cambridge, MA 02142; [2]Department of Developmental Biology, Harvard School of Dental Medicine, Boston, MA 02115; [3]Center for Craniofacial Regeneration, Department of Oral Biology, University of Pittsburgh, School of Dental Medicine, Pittsburgh, PA 15213; [4]Department of Biological Chemistry, Johns Hopkins University School of Medicine, Baltimore, MD 21205; [5]Department of Biologic and Material Sciences, University of Michigan School of Dentistry, Ann Arbor, MI 48108; [6]Center for Craniofacial Regeneration, Department of Periodontics and Preventive Dentistry, University of Pittsburgh, School of Dental Medicine, Pittsburgh, PA 15213

Running title: *Amelogenin phosphorylation is essential for enamel formation*

[%]Present address: Department of Pediatric Hematology-Oncology, Boston Children's Hospital and Dana Farber Cancer Institute, Harvard Medical School, 300 Longwood Ave, Boston, MA 02115

[#]Present address: Center for Craniofacial Regeneration, Department of Oral Biology, University of Pittsburgh, School of Dental Medicine, Pittsburgh, PA 15213

[&]Present address: Center for Craniofacial Regeneration, Department of Periodontics and Preventive Dentistry, University of Pittsburgh, School of Dental Medicine, Pittsburgh, PA 15213

*To whom correspondence should be addressed: Henry C. Margolis, Ph.D., Center for Craniofacial Regeneration, Department of Periodontics and Preventive Dentistry, University of Pittsburgh School of Dental Medicine, Pittsburgh, PA 15213, hmargolis@pitt.edu; Tel. (412) 648-8499; Fax. (412) 624-6685.

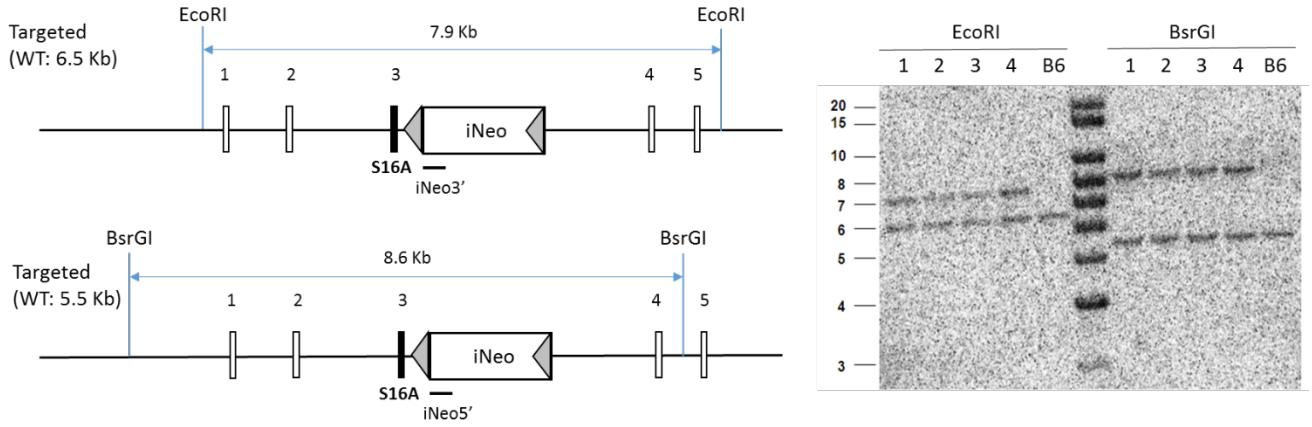

Figure S1. Secondary confirmation of positive clones identified by PCR was performed by Southern blot analyses. DNA was digested with EcoR I and BsrG I to confirm the integration targeting vector. The digested DNA was electrophoretically separated on a 0.8% agarose gel. After transfer to a nylon membrane, the digested DNA was hybridized with a probe (iNeo) targeted against the Neo Cassette. DNA from C57Bl/6 (B6) mouse strains were used as wild type controls. The expected sizes are indicated on the schematic. FRT sites are represented by gray triangles.

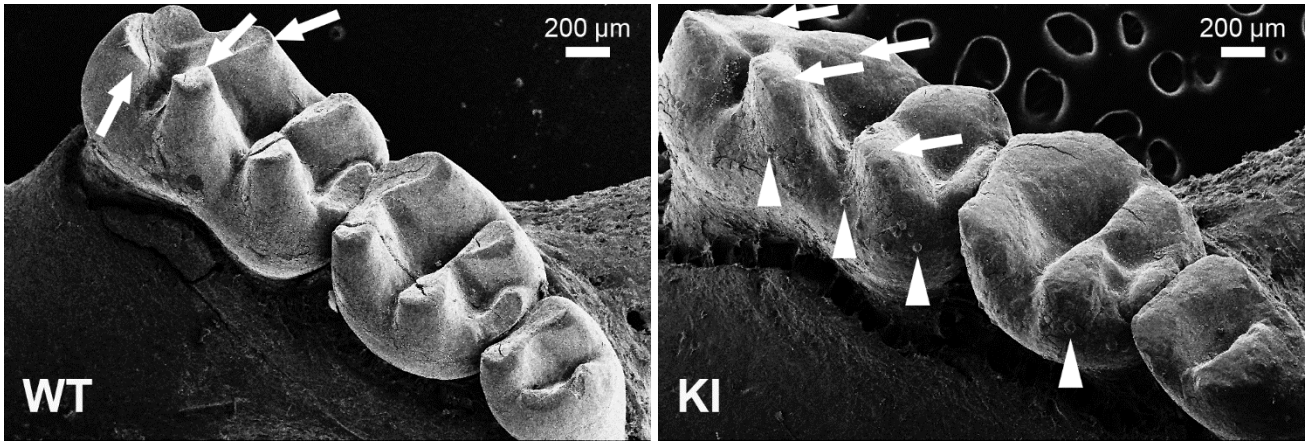

Figure S2. SEM analyses of WT and KI molars. WT molars exhibit smooth enamel surfaces, while large mineral nodules (arrowheads) are observed on KI enamel surfaces using SEM. As also indicated (arrows), KI molars cusps appear rounded in comparison to the sharp, chisel-like appearance of WT molar cusps, suggesting that KI cusp enamel is much thinner than that of the WT.

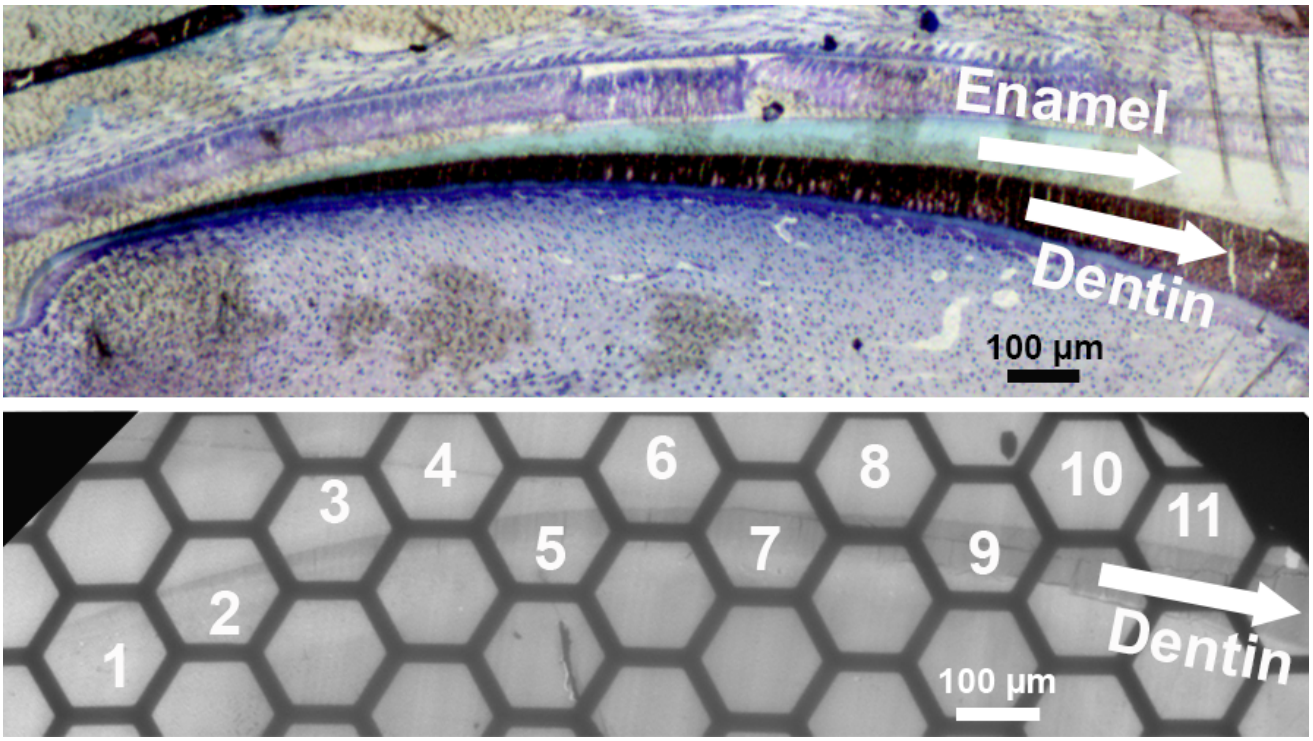

Figure S3. Illustration of how sequential stages of enamel development in WT, HET and KI TEM sections were identified for characterization. (**A**) The upper panel is an example of a low magnification light microscope image of a 1 mm thin section of developing enamel of a WT incisor stained with toluidine blue. Initial developmental stages of enamel, dentin, and ameloblast layers are clearly observed. (**B**) The lower panel is a TEM image of a 70-100 nm ultrathin section prepared from the same WT incisor sample shown above. The darker area observed is dentin. The less mineralized enamel structure is on top of the dentin layer, but cannot be seen at this low magnification. The sequential stages of enamel development in WT, HET and KI sections using TEM were identified for characterization, as follows. The grid spacings ("grids") that outline developing enamel structures are numbered sequentially starting from grid 1, where the developing enamel mineral structure first appears, and extending to the early maturation stage enamel that occurs at grids 12 or 13 (not visible in this example). The width (measured side to side) of each 'grid' is approximately 130 µm.

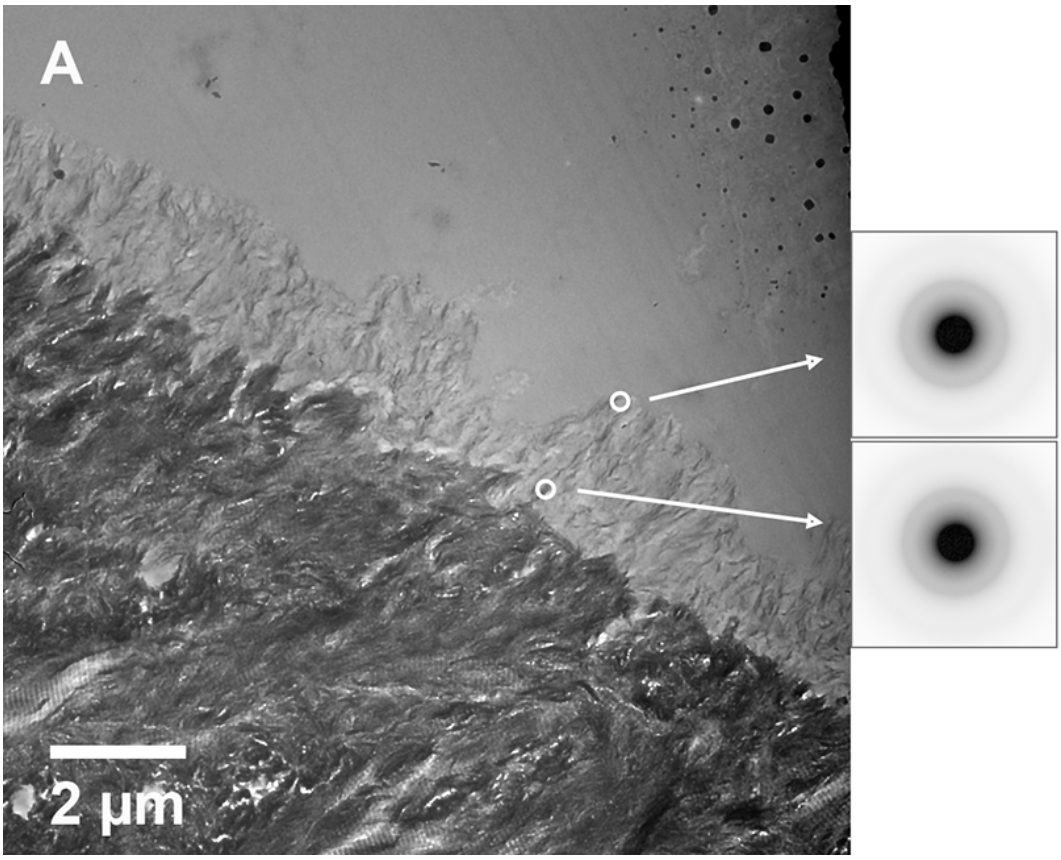

Figure S4A. TEM and SAED analyses of developing WT enamel. White circles represent the locations of SAED measurements. During the early secretory stage of enamel formation (grid 1) in WT enamel, a rodless enamel layer initially grows perpendicular to the DEJ to form a thin rodless (aprismatic) enamel layer on top of dentin. SAED results indicate that this thin mineral layer is amorphous (ACP) in nature. As shown, near both the enamel surface and the DEJ, within this thin aprismatic enamel layer, SAED results show a lack of distinct diffraction dots indicating that the enamel mineral phase is amorphous (ACP).

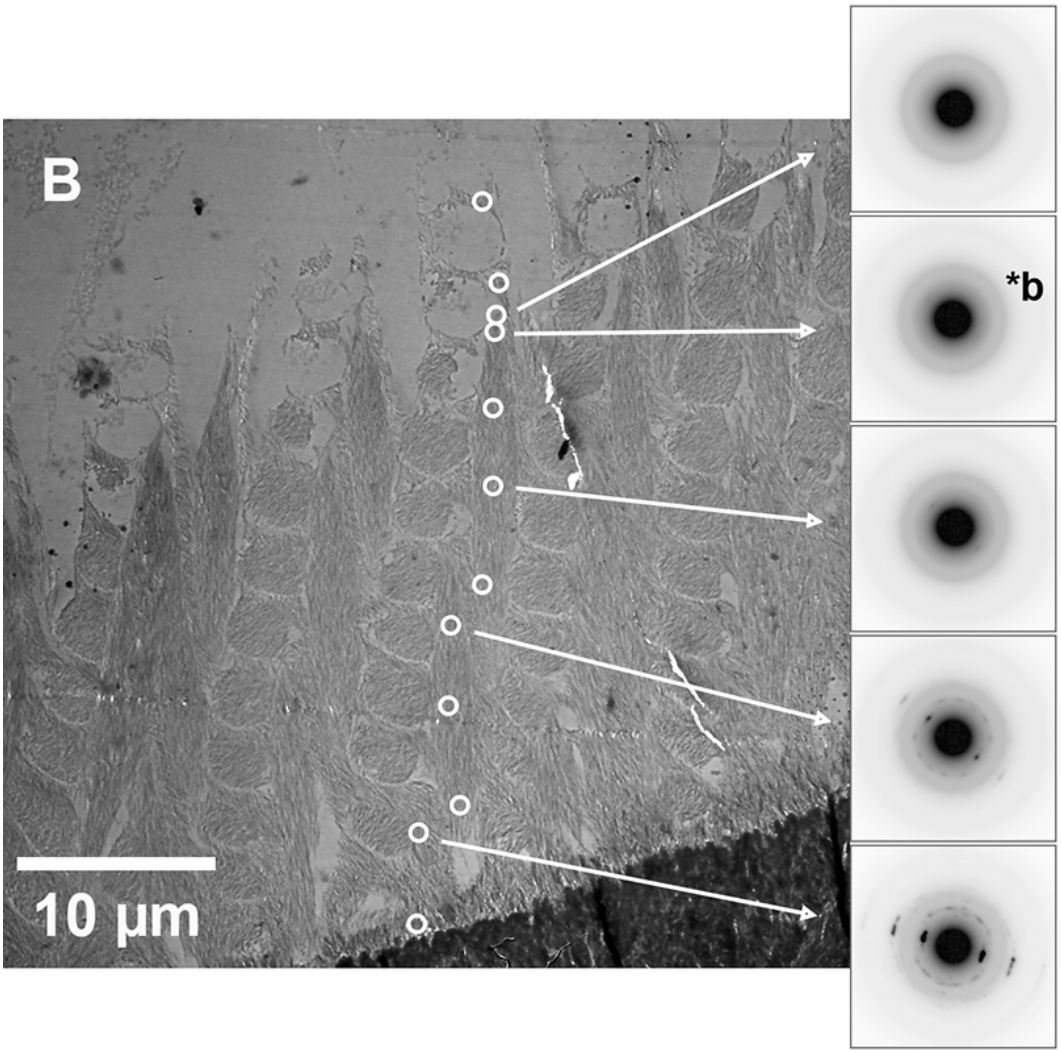

Figure S4B. TEM and SAED analyses of developing WT enamel. By the middle secretory stage (grid 5) in WT enamel, the enamel layer has grown thicker, and an enamel rod structure is clearly observed. From the enamel surface where newly deposited enamel is observed to the third location of SAED measurements (*i.e.*, the top SAED image on the right), distinct diffraction is again lacking indicating that the enamel mineral is amorphous at these locations. By the fourth measurement, however, faint diffraction dots start appearing indicating that the amorphous enamel particles are beginning to transform into crystals (see **Fig. S4G -*b** for a larger image). From this point on toward the DEJ where older enamel is found, a distinct diffraction pattern becomes clearer as measurements get closer to the DEJ. Near DEJ (the bottom SAED image), electron diffraction shows clear dots and an arc pattern that is consistent with the presence of well-aligned apatitic crystals, based on the presence of diffraction arcs from the 002 and 004 reflections of the c-axis of the HA crystal lattice structure with a narrow angular spread, as previously reported [1, 2].

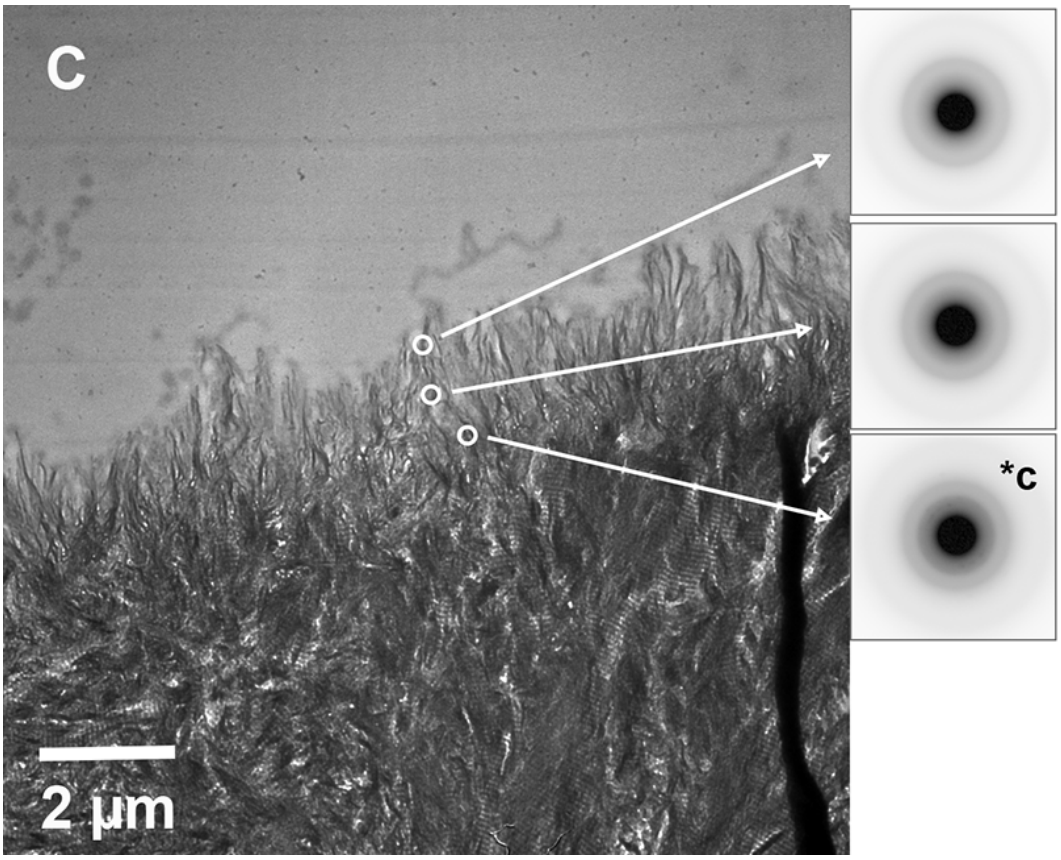

Figure S4C. TEM and SAED analyses of developing KI enamel. During the early secretory stage (grid 1) in KI enamel, a rodless enamel layer is again observed forming on top of a more densely mineralized dentin layer, as seen in WT enamel (**S4A**). As shown, two SAED measurements made in the outer portion of this thin enamel layer did not show evidence of electron diffraction, indicating that enamel mineral at these locations is amorphous, as similarly seen in WT enamel (**S4A**). Unlike WT enamel, however, faint SAED dots were observed (bottom SAED image) in older enamel near the DEJ (see **Fig. S4G -*c** for a larger image), suggesting that crystal formation had begun.

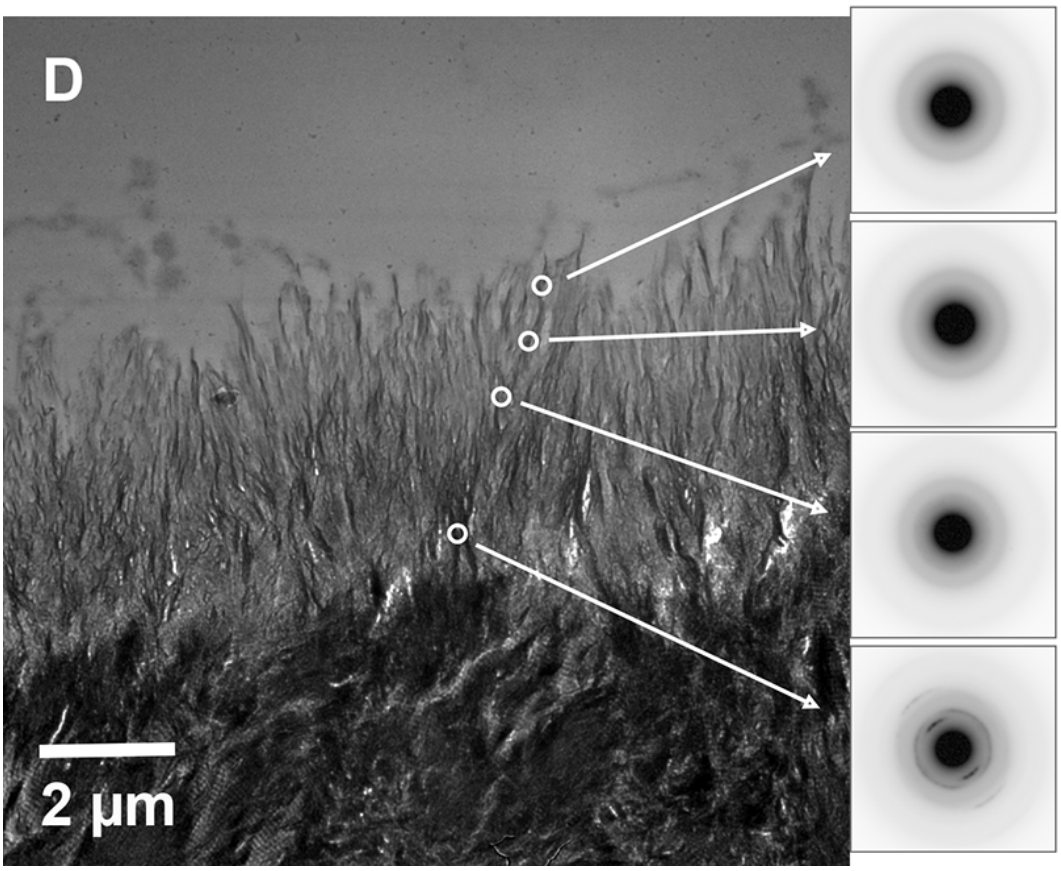

Figure S4D. TEM and SAED analyses of developing KI enamel. SAED results clearly show as KI development continues, as shown here at the beginning of grid 2 (**D**), clear evidence of electron diffraction is seen at the inner most measurement point.

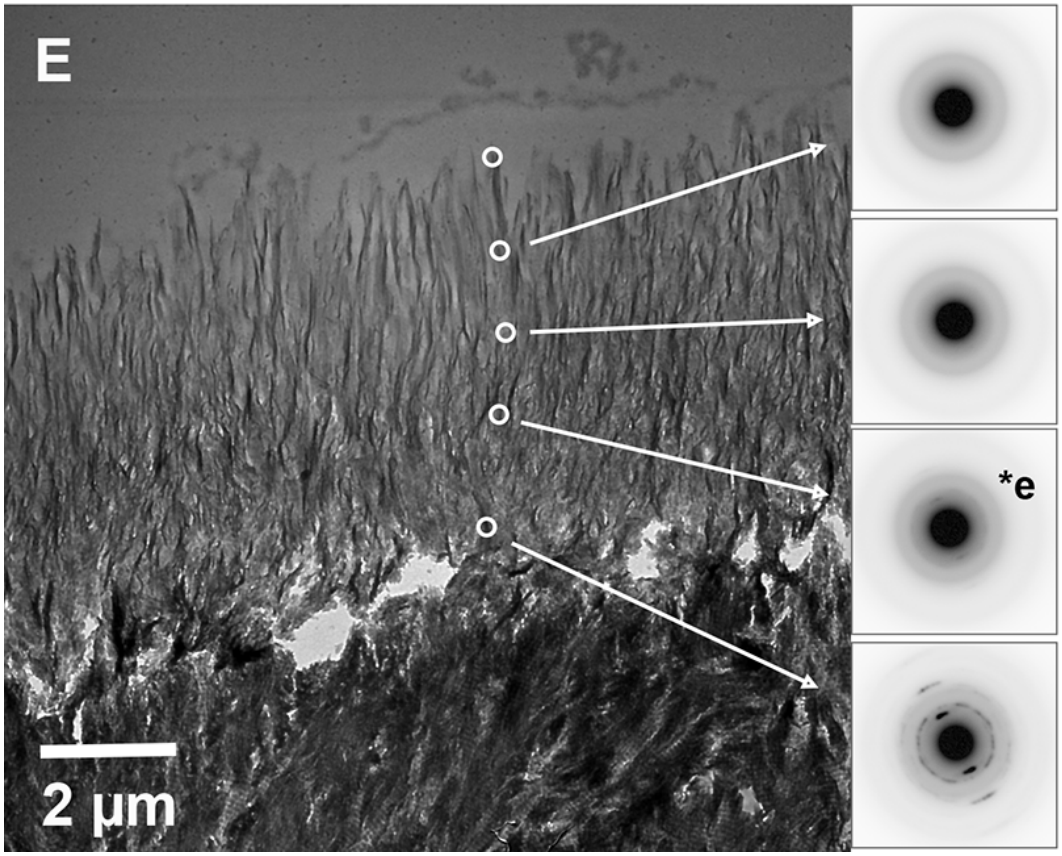

Figure S4E. TEM and SAED analyses of developing KI enamel. SAED results consistent with crystal formation are again more clearly seen as KI development continues, as shown at end of grid 2 (**E**). As shown, clear evidence of electron diffraction is seen in the inner two measurement points, respectively (see **Fig. S4G -*e** for a larger image). In grid 2 (**E**), we begin to see some breakage and loss of mineral above the DEJ in KI enamel.

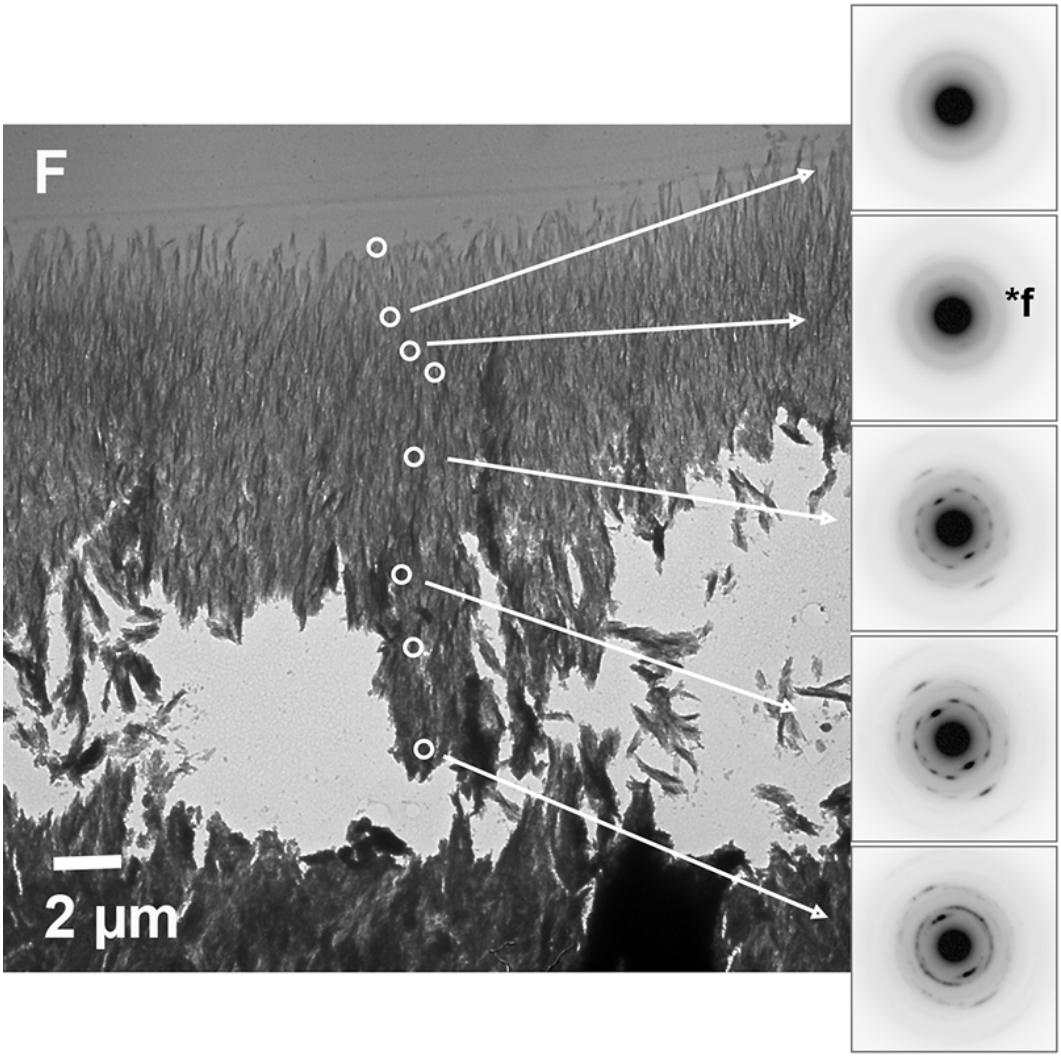

Figure S4F. TEM and SAED analyses of developing KI enamel. By the mid-secretory stage (grid 4) of KI enamel, and throughout the rest of enamel development, an enamel rod structure is not observed. As noted in the text, the mid-portion of the developing KI enamel matrix breaks away during TEM section preparation. However, we are able to carry out SAED measurements (white circles) in an approximately perpendicular direction from the enamel surface toward the DEJ, as was done with WT enamel samples. From the enamel surface to the location of the second SAED measurement (top SAED image), distinct diffraction patterns were not observed indicating that the KI enamel mineral particles are amorphous at these points. At the third measurement site, however, faint diffraction dots started to appear, indicating that amorphous enamel particles had begun to transform into enamel crystals (see **Fig. S4G -*f** for a larger image). From this point to the DEJ, diffraction patterns became clearer, as measurements were made closer to the DEJ. These SAED images (*e.g.,* the bottom SAED image) showed clear dot and arc patterns that are similar to those observed in WT enamel and also consistent with the presence of well-aligned enamel crystals, with a narrow angular spread of the 002 and 004 reflections of the c-axis of the HA crystal lattice structure.

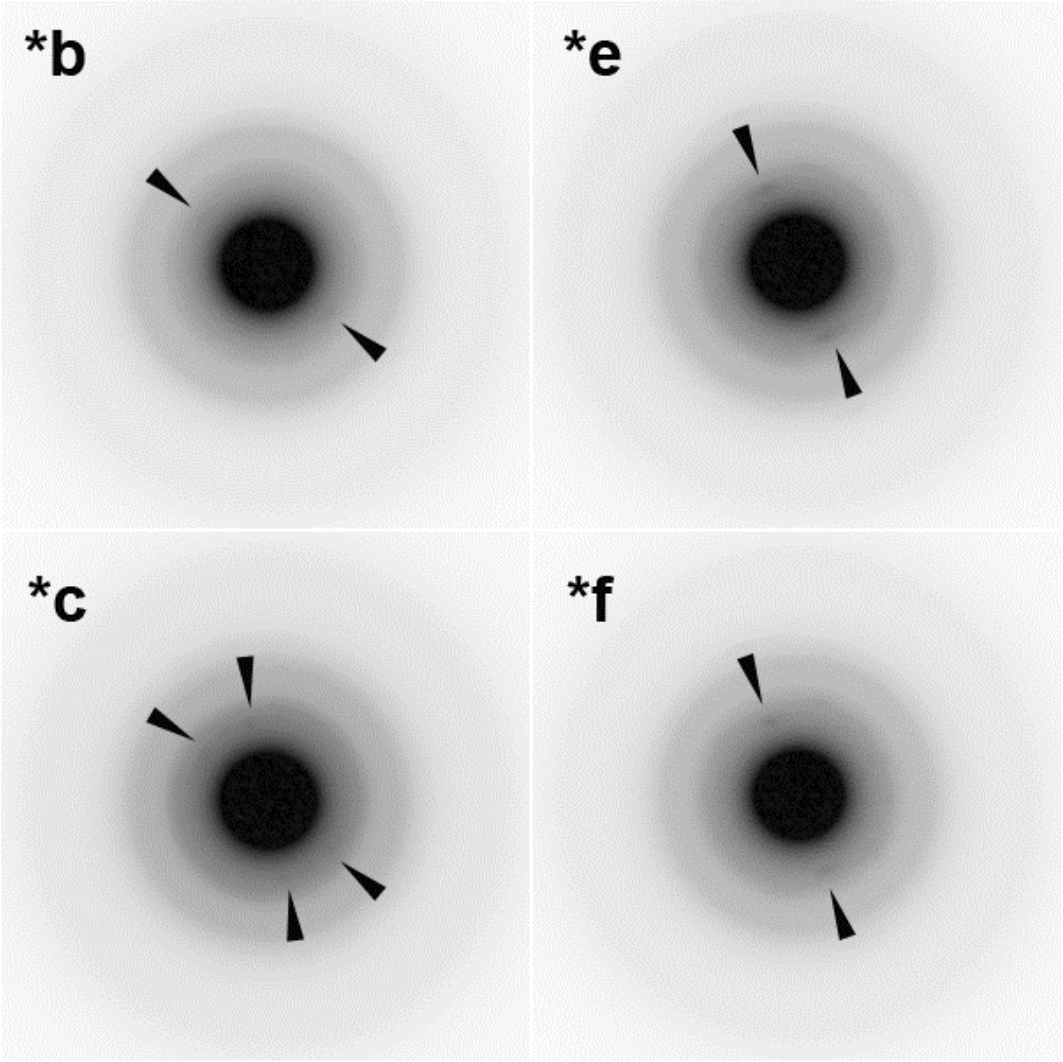

Figure S4G. Selected enlarged SAED images: (***b**) – Fig. S4B; (***c**) – Fig. S4C; (***e**) – Fig. S4E; and (***f**) – Fig. S4F, showing the presence of diffraction dots and arcs, consistent with the beginning of crystal formation.

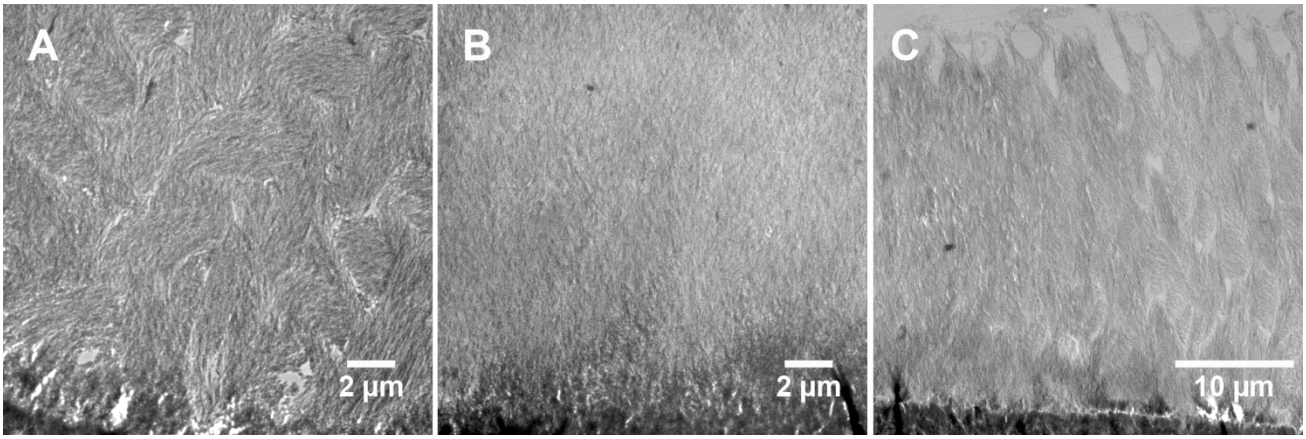

Figure S5. TEM images of the HET enamel matrix in the secretory stage illustrating the variability of its developing mosaic enamel phenotype. Samples of HET enamel can develop with a predominant WT-like (**A**) or KI-like appearance (**B**), or with an apparent mosaic structure (**C**) with clear rod-like features (to the right side) adjacent to an area that lacks this characteristic WT enamel structure, as shown. These images were obtained from different maxillary incisors of different mice.

References

1. E. Beniash, R.A. Metzler, R.S.K. Lam, P. Gilbert, Transient amorphous calcium phosphate in forming enamel, J Struct Biol 166 (2009) 133-143.

2. H. Yamazaki, B. Tran, E. Beniash, S.Y. Kwak, H.C. Margolis, Proteolysis by MMP20 Prevents Aberrant Mineralization in Secretory Enamel, J Dent Res 98 (2019) 468-475.